

UDC 669.721.5

<https://doi.org/10.17073/0021-3438-2023-1-39-55>

Research article

Научная статья



Investigation of castability, mechanical, corrosion properties and flammability of ML-OPB and EWZ43 magnesium alloys

V.E. Bazhenov¹, I.I. Baranov¹, A.A. Lyskovich¹, A.V. Koltygin¹, A.V. Sannikov¹,
K.A. Kyaramyan², V.D. Belov¹, S.P. Pavlinich²

¹ National University of Science and Technology “MISIS”

4 Leninskii pr., Moscow, 119049, Russia,

² Branch of JSC “United Engine Corporation”

Research Institute of Technology and Organization of Engine Production

16, build. 182 Budennogo av., Moscow, 105118, Russia

✉ Vyacheslav E. Bazhenov (V.E.Bagenov@gmail.com)

Abstract: Magnesium alloys are usually considered as structural materials when the weight reduction is important - in aircraft and space industry for example. In recent years, there has been an increase in the use of new generation ignition-proof high-strength magnesium alloys in the design of aircraft parts. The properties of new ignition-proof casting magnesium alloys ML-OPB (Mg–6.7Y–2.6Zn–0.5Zr–0.35Ce–0.35Yb; wt.%) and EWZ43 (Mg–3.8Y–4.4Nd–0.6Zr–0.6Zn; wt.%) were investigated and compared with properties of commercial magnesium alloys. The microstructure of investigated alloys in the as-cast condition comprises of a magnesium solid solution and a significant amount of eutectic. Heat treatment according to the T6 mode results in change in the eutectic phase’s morphology and also to their partial dissolution in the magnesium matrix. Long-term high-temperature holding, simulating operating conditions (500 h at 300 °C), leads to the formation of precipitates along the grain boundaries in both alloys, significantly reducing the mechanical properties. During the oxidation of the samples, it was established that the main components that involved into the oxide film and provides the protective properties of the alloys is Y, Nd and Yb. The investigated alloys have a high strength, which is not lower than that of the ML10 alloy. At the same time, the advantage of the ML-OPB alloy is a high elongation at fracture, while the EWZ43 alloy is characterized by high strength. The corrosion rate of the investigated alloys exceeds the corrosion rate of known commercial ML10 and AZ91 alloys, which implies the need for additional protection against corrosion of investigated alloys. At the same time, the castability of ML-OPB and EWZ43 alloys is no lower than that of most commercial magnesium alloys. An oxide film with high Y content and high protective properties is formed when the alloys interact with the sand mold bonded with furan resin. The ignition temperature of the investigated alloys is 100–150 °C higher than that of the ML10 alloy. The flammability test of alloys in the flame of a gas burner, made on cone samples and typical aircraft castings «bracket», showed that ML-OPB and EWZ43 alloys are almost non-flammable under the conditions of experiment.

Keywords: magnesium alloys, ignition temperature, corrosion resistance, mechanical properties, castability, ignition-proof

Funding: The work was undertaken as part of research project between JSC UEC and NUST MISIS.

For citation: Bazhenov V.E., Baranov I.I., Lyskovich A.A., Koltygin A.V., Sannikov A.V., Kyaramyan K.A., Belov V.D., Pavlinich S.P. Investigation of castability, mechanical, corrosion properties and flammability of the ML-OPB and EWZ43 magnesium alloys. *Izvestiya. Non-Ferrous Metallurgy*. 2023; 29 (1): 39–55. (In Russ.). <https://doi.org/10.17073/0021-3438-2023-1-39-55>

Исследование литейных, механических, коррозионных свойств и пожароопасности магниевых сплавов МЛ-ОПБ и EWZ43

В.Е. Баженов¹, И.И. Баранов¹, А.А. Лыскович¹, А.В. Колтыгин¹, А.В. Санников¹,
К.А. Кярамян², В.Д. Белов¹, С.П. Павлинич²

¹ Национальный исследовательский технологический университет «МИСИС»

119049, Россия, г. Москва, Ленинский пр-т., 4

² Филиал АО «Объединенная двигателестроительная корпорация»

АО Научно-исследовательский институт технологии и организации производства двигателей

(АО «ОДК» «НИИД»)

105118, Россия, г. Москва, пр-т Буденного, 16, корп. 182

✉ Вячеслав Евгеньевич Баженов (V.E.Bagenov@gmail.com)

Аннотация: Магниевые сплавы как конструкционные материалы обычно рассматриваются в тех случаях, когда снижение массы имеет важнейшее значение, например в авиации и космонавтике. В последние годы наблюдается расширение применения пожаробезопасных высокопрочных магниевых сплавов нового поколения в конструкциях авиационных изделий. В работе были изучены свойства новых пожаробезопасных литейных магниевых сплавов МЛ-ОПБ (Mg–6,7Y–2,6Zn–0,5Zr–0,35Ce–0,35Yb) и EWZ43 (Mg–3,8Y–4,4Nd–0,6Zr–0,6Zn) и выполнено их сравнение с промышленными магниевыми сплавами. Микроструктура исследуемых сплавов в литом состоянии представляет собой магниевый твердый раствор и значительное количество эвтектики. Термическая обработка по режиму T6 приводит к изменению морфологии фаз в эвтектике, а также их частичному растворению в магниевой матрице. В результате длительной высокотемпературной выдержки, имитирующей условия эксплуатации (500 ч при 300 °С), происходит формирование выделений по границам зерен в обоих сплавах, которые значительно снижают механические свойства. Было установлено, что при окислении образцов основными компонентами, переходящими в оксидную плену и обеспечивающими защитные свойства сплавов, являются Y, Nd и Yb. Рассматриваемые сплавы обладают высокими прочностными свойствами, которые не ниже, чем у сплава МЛ10. При этом преимущество сплава МЛ-ОПБ является высокое относительное удлинение, а для сплава EWZ43 характерна высокая прочность. Скорость коррозии этих сплавов выше, чем у известных промышленных сплавов МЛ10 и МЛ5, из чего следует, что исследуемые сплавы требуют дополнительной защиты от коррозии. При этом литейные свойства сплавов МЛ-ОПБ и EWZ43 оказались не ниже, чем у наиболее распространенных магниевых сплавов. При взаимодействии сплавов с формой из холодно-твердеющей смеси формируется оксидная пленка с высоким содержанием Y и хорошими защитными свойствами. Температура возгорания изученных сплавов оказалась на 100–150 °С выше, чем у сплава МЛ10. Испытание сплавов в пламени газовой горелки на конусных образцах и типовых авиационных отливках типа «кронштейн» показало, что сплавы МЛ-ОПБ и EWZ43 практически не горят в условиях эксперимента.

Ключевые слова: магниевые сплавы, температура возгорания, коррозионная стойкость, механические свойства, литейные свойства, пожаробезопасность

Финансирование: Работа выполнена в рамках НИР между АО «ОДК» и НИТУ МИСИС.

Для цитирования: Баженов В.Е., Баранов И.И., Лыскович А.А., Колтыгин А.В., Санников А.В., Кярамян К.А., Белов В.Д., Павлинич С.П. Исследование литейных, механических, коррозионных свойств и пожароопасности магниевых сплавов МЛ-ОПБ и EWZ43. *Известия вузов. Цветная металлургия*. 2023; 29 (1): 39–55. <https://doi.org/10.17073/0021-3438-2023-1-39-55>

Introduction

The creation of ignition-proof casting magnesium alloys represents a very urgent task, especially for the aircraft industry [1]. Currently, it is recognised as economically and technologically advantageous to expand the use of new generation of ignition-proof high-

strength magnesium alloys in the design of aircraft parts [2].

Ignition resistance is directly dependent on the ability of the oxide film on the surface of the magnesium alloys to protect the metal from contact with atmospheric

oxygen over a wide temperature range [3]. The protective properties of an oxide film can be evaluated by the Pilling—Bedworth ratio (P—B ratio), which indicates the ratio of the oxide volume to the metal volume. If it is greater than 1, the film forming on the surface of the alloy is dense and protects it well against further oxidation. For magnesium and its oxide, the value of P—B ratio is 0.81 [4], i.e., a dense film is not formed. However, with the addition of certain alloying elements the density of the oxide film on the surface of the alloys increases significantly. For example, for the yttrium/yttrium oxide pair, the P—B ratio is 1.39 [4], which means that if an oxide layer with a predominant composed of Y_2O_3 is present, it should be dense and protect the alloy well against oxidation and ignition. Yttrium can therefore be used as an alloying element for ignition-proof alloys. Other rare-earth metals (REs) also contribute to the formation of a protective oxide film. For example, the positive effect of yttrium [5] neodymium [6] lanthanum [7], cerium [8] is known. Calcium is another excellent choice as a component to enhance the protective properties of the oxide film. Numerous studies [9–11] indicate a significant increase in the ignition temperature in the alloys after the addition of calcium.

It is worth noting that the joint addition of several elements that increase the density of the oxide film provides the maximum protective effect. For instance, it was shown in works [5, 8] that the dense oxide film is formed on the surface of Mg—Y alloy when the Y content exceeds 10 wt.%. If a small amount of Ce is subsequently added to the Mg—Y alloy, however, a dense protective film can be formed even at 3 wt.% Y.

Known ignition resistant alloys of the Mg—RE—Zn—Zr system with additions of Sc and Cd, developed by VIAM (Moscow) [12]. The alloys exhibit good strength, high ignition temperatures and a density of less than 2 g/cm^3 . However, the addition of Cd poses environmental risks to the melting of this alloy, whereas Sc is a very expensive alloying element and is currently used industrially only as a microalloying element in aluminum alloys [13].

Earlier, the EWZ43 alloy of the Mg—Nd—Y—Zn—Zr system was developed at MISIS [14], which combines good mechanical properties with high castability [15]. Due to the high Y and Nd content, this alloy should exhibit a high resistance to ignition.

Togliatti State University (TSU) in cooperation with Solikamsk Experimental Metallurgical Plant (SOMZ) proposed the ML-OPB alloy, which is close to the $Mg_{97}Y_2Zn_1$ alloy in content of yttrium and zinc and additionally alloyed with small quantities of Ce and

Yb to increase the ignition temperature. $Mg_{97}Y_2Zn_1$ alloy belongs to alloys with the LPSO (long-period stacking-ordered) phase, usually used to obtain products by plastic deformation methods. Moreover, it is well studied [16–18]. At the same time in the as-cast condition the alloys of Mg—Y—Zn—Zr system can exhibit high mechanical properties (tensile yield strength (TYS) of 150–180 MPa), however, only in the presence of W phase ($MgYZn_2$ or $Mg_3Zn_3Y_2$) apart from the LPSO-phase in the alloy structure [19–21]. Thus, in this system the promising casting alloys with excellent castability and high resistance to ignition can be found.

The development of new ignition-proof alloys is quite an urgent task, however, designers need a thorough understanding of their properties in order to be able to offer such alloys. In this regard, the aim of this paper was to investigate the castability, mechanical properties, corrosion properties and flammability of EWZ43 and ML-OPB magnesium alloys and to compare them with the properties of currently used commercial magnesium alloys.

Materials and methods

The ML10 and ML-OPB alloys were supplied by SOMZ LLC (Solikamsk). Magnesium (99.9 wt.% purity), zinc (99.975 wt.%), and Mg—15wt.%Zr (SOMZ LLC), Mg—20wt.%Y and Mg—20wt.%Nd (Metagran LLC, Moscow) master alloys were used to prepare the EWZ43 alloy.

Samples for corrosion tests were obtained by flux-free melting. Melting in the PT 90/13 resistance furnace (LAC, Czech Republic) was carried out in a steel crucible in a protective atmosphere of argon mixture with 2 vol.% sulfur hexafluoride (SF_6). The weight of alloy charge was 2 kg. After the raw materials was melted and the temperature was raised to 740–760 °C, the melt was purged with argon for 3 min through a steel tube. The melt was poured into the molds at the same temperature after a 10-minute holding in the furnace.

All other samples were obtained by flux melting technology, which was conducted in an induction furnace (RELTEK RRE, Ekaterinburg) in a steel crucible. The weight of the alloy charge was 2–4 kg. Melting was carried out under a flux on the basis of carnallite ($KCl \cdot MgCl_2$). Once the raw materials had been melted, the melt temperature was raised to 740 °C and a carnallite flux was added to clean the melt from non-metallic inclusions. The finished melt was held in the furnace for 10 min and then poured into the molds at a temperature of 740 °C. The mold temperature was 25 ± 2 °C.

To study the alloy microstructure, corrosion resistance and flammability, cylindrical ingots 35 mm in diameter and 150 mm in height were cast in a steel mold.

The chemical composition of ML10 and ML-OPB alloys was taken from the alloy data sheets, and for the EWZ43 alloy it was determined by optical emission spectroscopy on the ARGON-5SF spectrometer (Spectrosoft LLC, Troitsk). The composition of the alloys is presented in Table 1.

The microstructure and phase composition of the alloys were studied using a Vega SBH3 scanning electron microscope (SEM) (Tescan, Czech Republic) with an energy dispersive X-ray microanalysis (EDS) attachment (Oxford, UK).

The phase composition of the alloys was calculated using the “Thermo-Calc 2016a” software (Thermo-Calc Software, Sweden) [22] with the TCMG4 thermodynamic database (TCS Mg-based Alloys Database version 4) [23].

All alloys were heat-treated (HT) according to the T6 regime consisting of solution HT ($t = 525\text{ °C}$ for $\tau = 24\text{ h}$ — ML-OPB; $t = 525\text{ °C}$, $\tau = 8\text{ h}$ — EWZ43; $t = 530\text{ °C}$, $\tau = 10\text{ h}$ — ML10) followed by quenching in water and aging ($t = 200\text{ °C}$, $\tau = 100\text{ h}$ — ML-OPB; $t = 250\text{ °C}$, $\tau = 9\text{ h}$ — EWZ43; $t = 200\text{ °C}$, $\tau = 8\text{ h}$ — ML10).

To determine the mechanical properties of the alloys, the rectangular ingots were made by casting in a graphite mold [24]. Six cylindrical specimens with 5 mm gauge diameter were obtained from ingots for the tensile tests by lathing. The tensile test was conducted on the 5569 universal testing machine (Instron, USA) with an advanced video extensometer (Instron, USA).

Besides the mechanical properties in the HT-state, the mechanical properties after a long-time elevated temperature holding of the alloy samples at $t = 300\text{ °C}$ for 500 h were determined. The crucibles with samples were held in a forced-air furnace that provided both mixing of air inside the furnace and supply of new portions of air. The air flow velocity was measured with a 405i thermo-anemometer (Testo, Germany) and

was 0.06–0.2 m/s. The dimensions of the samples are shown in Fig. 1, *a*. Tensile tests were carried out on 3 specimens which had not been held out (in the HT state) and 3 specimens which had been held out at high temperature.

Samples for corrosion testing were cut from ingots using wire cutting. Corrosion tests were performed on cubic samples with dimensions of $12 \times 12 \times 12\text{ mm}$ and a surface area of approx. 9.5 cm^2 . The corrosion rate was determined by the volumetric method based on measuring the amount of hydrogen released during corrosion. The tests were performed in a 3 wt.% NaCl aqueous solution at room temperature for 48 h. The volume of the solution was 500 mL. Prior to immersion in the corrosion environment, the surface of the samples was

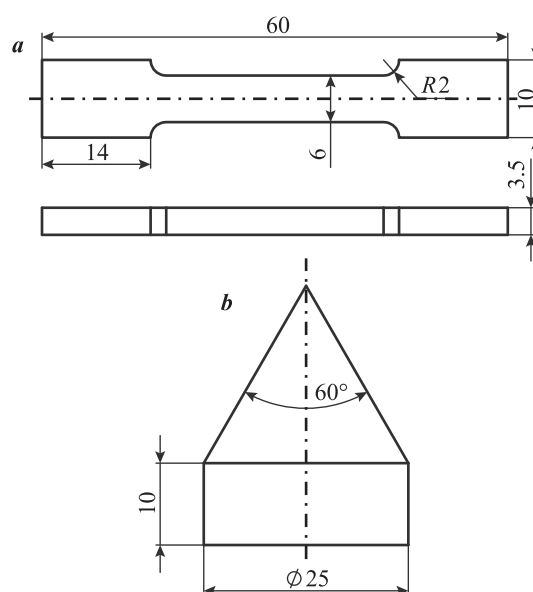


Fig. 1. The tensile test sample after longtime holding at elevated temperature (*a*) and a conical sample for alloy ignition testing in a gas burner flame (*b*)

Рис. 1. Образец для испытаний на растяжение после длительной выдержки при повышенной температуре (*a*) и конусный образец для проведения испытаний на возгорание сплава в факеле газовой горелки (*b*)

Table 1. The composition of investigated alloys, wt.%

Таблица 1. Состав исследуемых сплавов, мас.%

Alloy	Mg	Y	Nd	Zn	Zr	Ce	Yb
ML-OPB	Bal.	6.67	–	2.62	0.46	0.35	0.35
EWZ43	Bal.	3.76	4.39	0.63	0.58	–	–
ML10	Bal.	–	2.36	0.27	0.51	–	–

grounded with P320 grit sandpaper and degreased with ethyl alcohol. The amount of released hydrogen was converted into the mass loss of the sample according to the ratio of $1 \text{ mL H}_2 = 1 \text{ mg Mg}$ [25] and the corrosion rate was calculated in mm/year using the standard method [26].

Electrochemical studies for alloys in a 3 wt.% NaCl aqueous solution were performed using an IPC PRO MF/FRA potentiostat/galvanostat (Volta STC, St. Petersburg) at room temperature ($25 \pm 2 \text{ }^\circ\text{C}$). Measurements were performed in a three-electrode cell in which the alloy sample was the working electrode with an effective area of 1.6 cm^2 . Platinum and saturated silver/silver chloride (Ag/AgCl) electrodes were used as counter and reference electrodes, respectively. Potentiodynamic polarization experiments were performed from the cathode region at -2300 mV to the anode region at $+(1300+500) \text{ mV}$ at a scan rate of 1 mV/s . The corrosion current density and corrosion potential were determined using Tafel curves. Using the values of corrosion current density, the corrosion rate of the alloys was calculated [27]. Electrochemical measurements were repeated three times for each alloy.

The study of the fluidity of alloys was carried out with a spiral fluidity test. The molds for pouring the spiral test were made of resin bonded sand. For mold production according to “no-bake” process, the FK-5 binder and the OK-3 catalyst were used in the amount of 1.2 and 0.5 % of the sand mass (both produced by “Intema Group”, Pushkino, Russia), respectively. Quartz sand (deposit — Ryazan region) was used. The ignition inhibitor was potassium tetrafluoroborate (KBF_4) added in the amount of 0.5 % of the sand.

The mixture was prepared in a Mieszarki RN12/VL2 mixer (Multiserw-Morek, Poland). First the sand and ignition inhibitor were mixed, then the catalyst and, after it was evenly distributed, the binder were added to the mixture. After introducing each of the components, the mixture was mixed for 2 min.

Before pouring, the casting mold was aligned horizontally with a bubble level to determine fluidity. A wooden stopper was placed in the pouring cup, blocking the sprue. Melt was poured into the cup of the mold at $790\text{--}810 \text{ }^\circ\text{C}$ ($50\text{--}60 \text{ }^\circ\text{C}$ above the temperature at which the fluidity was determined). After filling the cup with melt, the temperature changes on the thermocouple located in the cup center were monitored. As soon as the temperature of the thermocouple reached the pouring temperature of $740 \text{ }^\circ\text{C}$ (after 5–15 s), the stopper was lifted. The spiral fluidity test was repeated 4 times. The temperature was monitored using the BTM-4208SD 12-channel temperature re-

corde (Lutron, Israel). K-type thermocouples were used.

The hot tearing susceptibility test was carried out in the molds made of resin bonded sand. The melt was poured into the molds at $780\text{--}800 \text{ }^\circ\text{C}$. The maximum ring width (in mm) at which a crack was detected was considered as a measure of hot tearing susceptibility (HTS), assuming that no cracks were detected at subsequent rings of greater width. The width of the poured rings ranged from 5 to 25 mm in increments of 2.5 mm. For each ring width, 2–4 probes were poured. Also the HTS of the alloys was determined by the “Dog-bone” test. The sample as a casting has a massive sprue with side branches of different lengths, but with the same cross-sectional area [29]. The end of each branch ended with a ball-shaped thickening, creating a hindered contraction. The “Dog-bone” probe was poured into a steel mold with a vertical parting line. The HTS of the alloys was assessed by the maximum branch length without cracks. 4 probes were poured for each alloy at a casting temperature of $740 \text{ }^\circ\text{C}$.

To determine the influence of the mold material on the surface quality of the castings, two castings of different configurations were made. The first represented bars with thickness 10, 20 and 30 mm, connected by a gating system — its scheme is presented in a work [28]. The second casting was a cylinder 60 mm in diameter and 135 mm length. Two types of resin bonded sand mixtures, with and without ignition inhibitor addition, were used to manufacture the mold for cylinder casting. Potassium tetrafluoroborate (KBF_4) was used as an ignition inhibitor in the amount of 0.5 % of the sand mass. No ignition inhibitor was used to obtain castings with bars of varying thickness. The nature of interaction between the alloy and the mold material and the effect of inhibitors on this interaction were evaluated visually by the surface quality of the castings obtained.

To determine the ignition temperature, rectangular samples of $10 \times 10 \times 5 \text{ mm}$ were cut from ingots. Their surfaces were grounded with P400 grit sandpaper. A hole 1.5 mm in diameter and 3–5 mm deep was drilled in each sample, into which the junction of a K-type thermocouple was mounted.

During the tests, alloy samples were placed in a steel crucible. Using an induction furnace, they were heated at a constant rate of $5 \text{ }^\circ\text{C/s}$. The ignition temperature of the alloy was determined by a sharp increase in the temperature on the heating curve, and visually by the appearance of flashes on the surface of the melted sample.

Cone-shaped samples were turned from ingots on a lathe for ignition test of the alloy in the gas burner flame (Fig. 1, *b*). The sample was placed on a sheet of asbestos with the tip upwards. The junction of a K-type thermocouple mounted on a tripod was placed 1–2 mm away from the tip of the cone to fix the flame temperature in the area of the cone tip. The flame of the gas burner was directed at the tip of the cone and a countdown began, simultaneously recording the temperature of the flame, which was approx. 1300 °C. In the course of the experiment the time to the appearance of the ignition source was visually recorded.

The molds for producing the “Bracket” casting were made using 3D printing. The molds were made using the Binder jetting technology using an SP 500 3D printer (Additive Technologies LLC, St. Petersburg). We used a furan-based BindEX+ binder (Prom-KhimTech LLC, Ivanteevka, Russia). The castings made of the ML-OPB, EWZ43 and ML10 alloys were casted in the printed molds.

A gas burner was placed in a specially prepared chamber made of refractory bricks, which provided a persistent flame for a long period of time. The casting was placed at a fixed distance from the burner, ensuring its presence in the flame. The temperature of the flame at the casting location was recorded using a K-type thermocouple and was ~1100 °C. The purpose of the test is to record the time until at least one ignition source has appeared.

Results and discussion

Figure 2, *a–c* represents the microstructure of the ML-OPB alloy. In the as-cast state (Fig. 2, *a*) in the structure of the alloy in addition to the primary dendrites of the magnesium solid solution α -Mg there is a significant amount of eutectic phase, which, according to the results of EDS analysis, has the composition, at.%: Mg–3.9Zn–6.2Y–0.42Zr–0.26Ce–0.09Yb. Based on the calculations performed with ThermoCalc, this phase is an LPSO-phase (Mg_{12}ZnY or $\text{Mg}_{21}\text{Zn}_2\text{Y}_2$). The precipitates in the center of the grains are zirconium based solid solution α -Zr. Heat treatment of the ML-OPB alloy leads to a change in the morphology of the LPSO-phase to lamellar as well as the formation of zirconium-rich needle precipitates in the center of the grain (Fig. 2, *b*). The long-time holding at elevated temperature causes the formation of tiny precipitates at grain boundaries. Due to their small size it is impossible to determine the composition of this phase, however, according to the EDS the precipitates of this phase are rich in Y and Zn.

Fig. 2, *d–f* shows the microstructure of the EWZ43 alloy in the as-cast and heat-treated states, as well as after long-time holding at elevated temperature for 500 h. Earlier in paper [15], the phase composition of this alloy was investigated and it was revealed that in the as-cast state in the structure of the alloy in addition to the α -Mg there is the eutectic Mg_3Nd phase, which transforms into the $\text{Mg}_{41}\text{Nd}_5$ phase after the HT. Long-time holding at elevated temperature, as in the case of the ML-OPB alloy, causes the formation of tiny precipitations located on the grain boundaries. The precipitates are enriched in Y and Nd according to the results of the EDS.

Fig. 3, *a* provides the tensile properties of the ML-OPB and EWZ43 alloys in the HT condition. The data for the EWZ43 alloy are taken from work [15] for two aging temperatures (200 and 250 °C). The tensile properties of the ML10 alloy are also given for comparison [30]. The ML-OPB alloy exhibits sufficiently similar tensile yield strength (TYS) and ultimate tensile strength (UTS) values to those obtained for the ML10 alloy, but with a significantly higher elongation at fracture (El). For the EWZ43 alloy, the maximum values of TYS and UTS are observed, but the minimum value of El among the materials is under consideration.

Fig. 3, *b* represents the tensile properties of the ML-OPB and EWZ43 alloys prior to and after long-time holding at elevated temperature. Since the tests in this case were performed on samples of a different configuration with a small cross-sectional area (see Fig. 1, *a*), they cannot be compared with the results of tensile tests obtained on full-size standard samples (Fig. 3, *a*). It can be seen that the ML-OPB and EWZ43 alloys show a significant decrease in TYS and UTS after a long-time holding at elevated temperature. The reduction in El for the ML-OPB alloy is especially significant (~50 %). At the same time, El for the EWZ43 alloy remains practically unchanged. Previously, it was pointed out in microstructure analysis that long-time holding at elevated temperature leads to phase precipitation along the grain boundaries, and it seems that these precipitations, as well as the loss of lattice coherence between the α -Mg and the precipitates released during ageing, cause a decrease in the mechanical properties.

After the long-time holding at elevated temperature, the oxide layer on the surface of the ML-OPB and EWZ43 alloy samples was investigated. Its element content, based on the EDS results, is provided in Table 2. It can be seen that during oxidation of the ML-OPB alloy sample, Y constitutes the main ele-

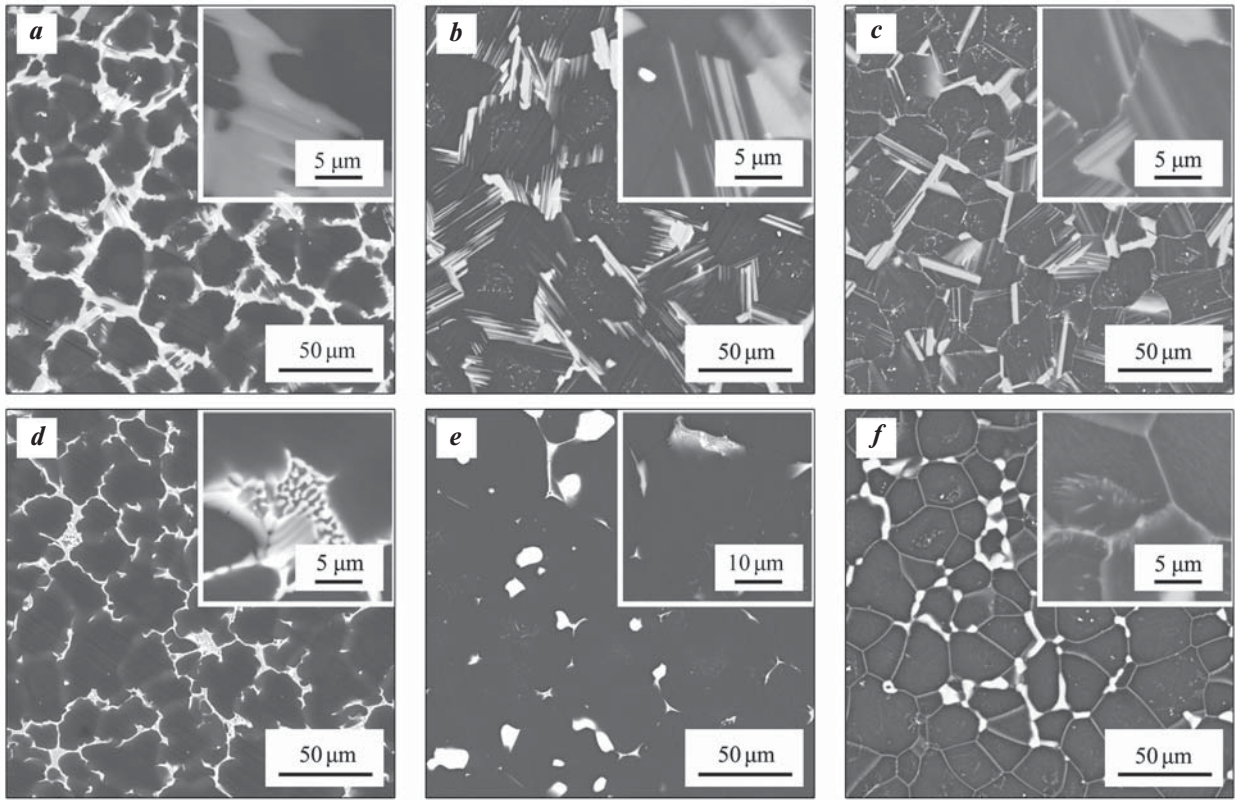


Fig. 2. Microstructure of ML-OPB alloy (a–c) and EWZ43 (d–f) in as-cast condition (a, d), heat-treated condition (b, e), and after longtime holding at elevated temperature (c, f)

Рис. 2. Микроструктура сплавов МЛ-ОПБ (a–c) и EWZ43 (d–f) в литом (a, d) и термообработанном (b, e) состояниях, а также после длительной высокотемпературной выдержки (c, f)

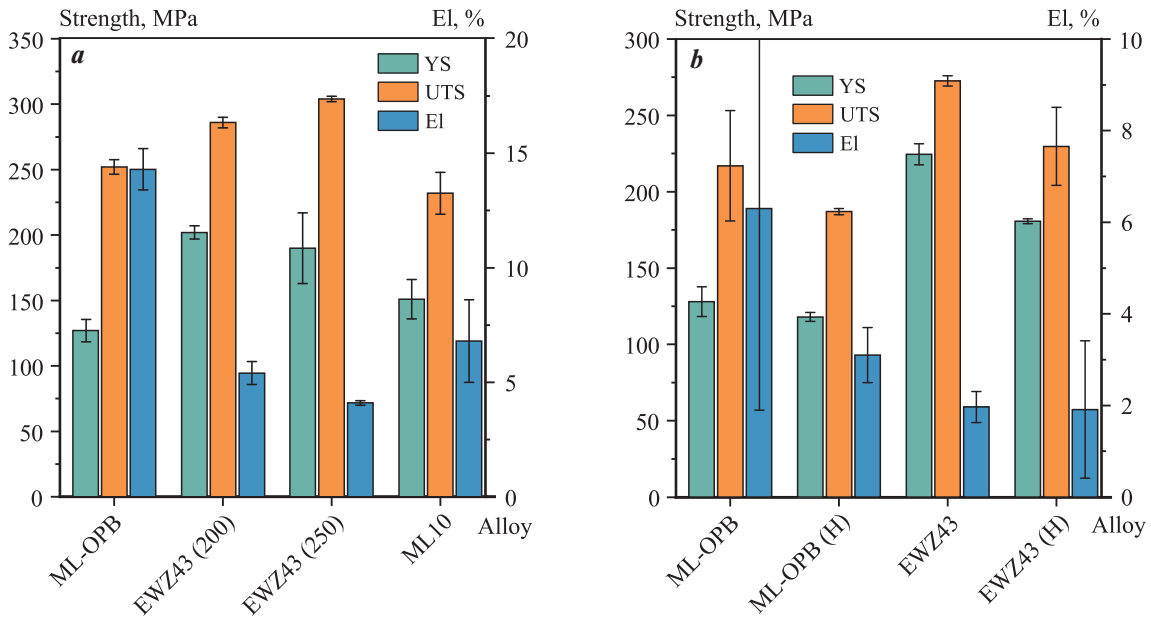


Fig. 3. Tensile properties of ML-OPB, EWZ43, and ML10 alloys after heat treatment (in parentheses the aging temperature of the EWZ43 alloy is indicated) (a), as well as the tensile properties of ML-OPB and EWZ43 alloys before and after longtime holding at elevated temperature (indicated by the B) at $t = 300$ °C for 500 h (b)

Рис. 3. Механические свойства при растяжении сплавов МЛ-ОПБ, EWZ43 и МЛ10 в термообработанном состоянии (в скобках указана температура старения сплава EWZ43) (a), а также сплавов МЛ-ОПБ и EWZ43 до и после длительной высокотемпературной выдержки (с буквой В) при $t = 300$ °C в течение 500 ч (b)

ment comprising the oxide film apart from Mg. There is also a higher Yb content in the oxide film than in the alloy. Regarding the other alloying elements of the ML-OPB alloy (Zn, Zr and Ce), their concentration in the oxide film is much lower than that observed in the alloy.

The predominant elements for the EWZ43 alloy whose content in the oxide layer is higher than that in the alloy are Y and Nd. The rest of the alloying elements are contained in the film either in close or much lower quantities than in the alloy.

Thus, such elements as Y (for both alloys), Nd (for the EWZ43 alloy), and Yb (for the ML-OPB alloy) play a protective role in the oxidation of the ML-OPB and EWZ43 alloys. The thickness of the surface oxide layer after a long-time holding at elevated temperature was from 10 to 30 μm for both alloys, indicating their high heat resistance at $t = 300\text{ }^\circ\text{C}$.

Fig. 4, *a* shows the amount of released hydrogen during corrosion tests of the ML-OPB and EWZ43 alloys in a medium of a 3 wt.% NaCl aqueous solution. It should be noted that during the tests, the intensity of hydrogen release for the ML-OPB alloy increases with time, while for the EWZ43 alloy it is almost constant. This pattern is not common in less-alloyed magnesium alloys. For comparison, the results of similar corrosion tests with the ML10 alloy from work [31] were added in Fig. 4, *a*. It can be seen that the corrosion rate is steadily decreasing due to the protective effect of the layer of corrosion products formed on the alloy surface.

Typical polarization curves for the ML-OPB and EWZ43 alloys obtained in a 3 wt.% NaCl aqueous solution are shown in Fig. 4, *b*. The average values of the corrosion potential, the corrosion current density and the calculated corrosion rate of the alloys under investigation, as determined from the polarization curves, are presented in Table 3. The values of these parameters

for the ML5 alloy obtained under similar conditions are also included in this Table [32]. It can be seen that the corrosion potential of the ML-OPB and EWZ43 alloys is almost the same and it is much more negative than that of the AZ91 alloy. At the same time, the corrosion current density is lower for the ML-OPB alloy compared to the EWZ43 alloy, and it is maximum for the AZ91 alloy.

Based on the results of hydrogen release corrosion tests and electrochemical research, the corrosion rates of the alloys were calculated (see Table 3). It can be seen that the corrosion rate determined from the electrochemical corrosion tests for the ML-OPB and EWZ43 alloys is much lower than that determined in the long-term immersion corrosion tests (by hydrogen release). In general, the corrosion rate for the alloys under investigation, calculated in hydrogen release tests, is 3–4 times higher than for the most common used commercial magnesium alloys (AZ91 and ML10).

Typically, the corrosion rate determined by Tafel fitting of polarization curves is equal to or lower than the corrosion rate determined by long-term immersion test (by hydrogen release), in particular, this pattern can be observed for the AZ91 alloy (Table 3). This is due to the fact that during the corrosion process, the resulting corrosion products cover the surface of the sample and thus prevent its contact with the corrosive environment. A possible reason to explain the increasing corrosion rate of the ML-OPB alloy as the corrosion process occurs is due to the microstructure of the alloy under investigation (see Fig. 2, *b*). Thus, the LPSO phase, which serves as cathode with respect to the α -Mg, is found in a structure in the form of coarse plates. During the corrosion process, the α -Mg dissolves and the surface area of the cathode phase increases [33], which leads to an increase in the corrosion rate.

Fig. 5 represents the values of fluidity obtained by the spiral test, hot tearing susceptibility (HTS) obtained

Table 2. The elements content at the surface of ML-OPB and EWZ43 alloys samples after longtime holding at elevated temperature obtained by Energy-dispersive X-ray spectroscopy

Таблица 2. Содержание элементов в оксидной пленке образцов сплавов МЛ-ОПБ и EWZ43 после длительной высокотемпературной выдержки по результатам РСМА

Alloy	Content, at.% / wt.%								
	Mg	Y	O	C	Nd	Zn	Zr	Ce	Yb
ML-OPB	65.8/59.3	6.4/21.3	21.0/12.5	5.9/2.6	–	0.18/0.43	0.18/0.59	0.10/0.53	0.39/2.47
EWZ43	58.1/53.1	4.9/16.4	28.9/17.4	5.9/2.7	1.7/9.4	0.05/0.13	0.16/0.54	–	–

Table 3. Results of electrochemical corrosion tests and hydrogen evolution corrosion tests for ML-OPB, EWZ43, ML10 and AZ91 alloys

Таблица 3. Результаты электрохимических коррозионных испытаний и коррозионных испытаний по выделению водорода для сплавов МЛ-ОПБ, EWZ43, МЛ10 и МЛ5

Alloy	Electrochemical corrosion tests			Corrosion tests by hydrogen release
	Corrosion potential, V	Corrosion current density, $\mu\text{A}/\text{cm}^2$	Corrosion rate, mm/year	Corrosion rate, mm/year
ML-OPB	-1.53 ± 0.03	74.4 ± 6.9	1.69 ± 0.16	6.93 ± 0.39
EWZ43	-1.56 ± 0.03	94.2 ± 26.5	2.12 ± 0.60	6.27 ± 1.05
ML10 [31]	–	–	–	0.95 ± 0.14
ML5 [32]	-1.42 ± 0.02	115.4 ± 20.8	2.47 ± 0.45	2.10 ± 0.08

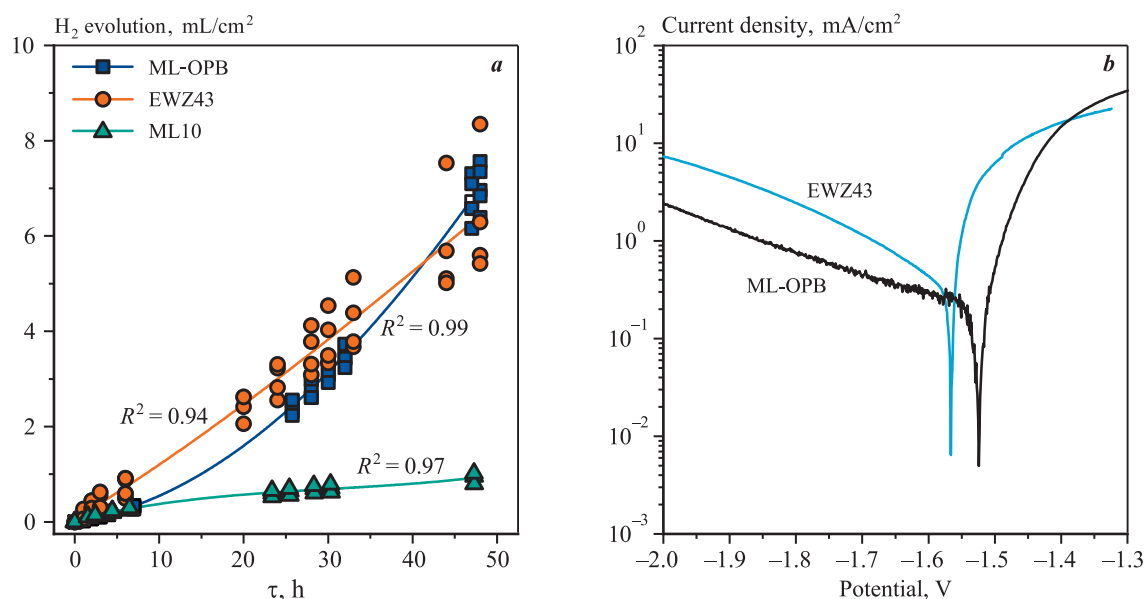


Fig. 4. The amount of hydrogen released during corrosion testing of ML-OPB, EWZ43, and ML10 alloys in a 3 wt.% NaCl aqueous solution (a) and polarization curves for ML-OPB and EWZ43 alloys in a 3 wt.% NaCl aqueous solution (b)

Рис. 4. Количество выделившегося водорода в ходе коррозионных испытаний сплавов МЛ-ОПБ, EWZ43 и МЛ10 в среде 3 мас. %-ного водного раствора NaCl (a) и поляризационные кривые для сплавов МЛ-ОПБ и EWZ43 в среде 3 мас. %-ного водного раствора NaCl (b)

by the ring and “Dog-bone” tests of the ML-OPB and EWZ43 alloys at a pouring temperature of 740 °C. It can be seen that the value of fluidity of the EWZ43 alloy coincides with that obtained for the AZ91 alloy (it was determined under similar conditions [32]), and the ML-OPB alloy exceeds the fluidity of these alloys (Fig. 5, a). It seems that the maximum fluidity of the ML-OPB alloy under consideration is associated with a large amount of eutectic in its structure, as well as with

a fairly short freezing range of alloys with the LPSO-phase [21].

Fig. 5, b shows the results of determining the HTS of alloys by the ring test. There are no confidence intervals for a number of alloys since there was a high degree of reproducibility of the results and for each ring width all three castings showed the same result. For the ML-OPB and EWZ43 alloys, the HTS, which indicates the maximum ring width at which the crack

appears, was found to be 15 and 17.5 mm, respectively. At the same time, according to OST (Industrial Standard) 1 90020-71 the HTS for the industrial AZ91 alloy is 30 mm. That is, the resistance to formation of hot cracks in the studied alloys is significantly higher than that of the AZ91 alloy. The reason for this is most likely that the AZ91 alloy exhibits a rather long freezing range, whereas the ML-OPB and EWZ43 alloys have a fairly short freezing range, moreover, their structure contains more eutectic. Because of the relatively short freezing range, the HTS of the ML10 alloy, according to OST (Industrial Standard) 1 90020-71, is 15–20 mm, i.e. comparable to the alloys under investigation. Also, the low HTS of the ML-OPB and EWZ43 alloys is promoted by the fine grain size, which is ensured by the presence of zirconium in the alloy [34].

Fig. 5, *c* represents the HTS values for the ML-OPB, EWZ43 and ML10 alloys obtained by the “Dog-bone” test. For the ML-OPB alloy, a complete absence of cracks was observed, indicating minimal HTS. The maximum crack-free branch length for the AZ91 alloy was 50 mm [32], which confirms the conclusions that the tendency to form hot cracks in the ML-OPB alloy is much lower than in the most common commercial cast magnesium alloy — AZ91. The EWZ43 alloy occupies an intermediate position between the specified alloys.

Rectangular bar castings with various thicknesses of the ML-OPB and EWZ43 alloys were poured into the molds made of resin bonded sand. The element content in the oxide film of the bars as determined by EDS

is shown in Fig. 6. The oxide film in all cases mainly contains C, O, Mg, and Y. The content of C in Fig. 6 is not given and can be calculated as a difference between 100 % and the contents of the other elements shown in the charts. In the MgO—Y₂O₃ system no ternary phases are formed [35], therefore it can be assumed that the film structure is composed of a mixture of MgO and Y₂O₃ phases. The ratio of Mg to Y in the film depends on the thickness of the bar. Thus, for a 10 mm thick bar, the magnesium content in the film is higher than the yttrium content, whereas in 20 and 30 mm thick bars the situation is reversed and the yttrium content is 1.5–2.0 times higher than that of magnesium. The quantitative ratio of the phase fractions cannot be established because the thickness of the film is shallow and the alloy of the bar under oxide layer affects the analysis result. That is, the higher magnesium content in a 10 mm thick bar is related to the fact that it bears a thinner oxide film. The composition of the oxide film for the ML-OPB and EWZ43 alloys is quite similar. The only difference is in the presence of a small amount (less than 1 at.%) of Nd in the EWZ43 alloy film. The remaining alloying elements (Zn, Zr, Ce and Yb) are virtually absent in the oxide film and do not affect the interaction of the ML-OPB and EWZ43 alloys with the resin bonded sand.

On the surface of cylindrical ingots with a diameter of 60 mm, after pouring into the molds without a ignition inhibitor in the resin bonded sand, separate areas of metal-mold interaction are observed, which is expressed as the appearance of defects in the form

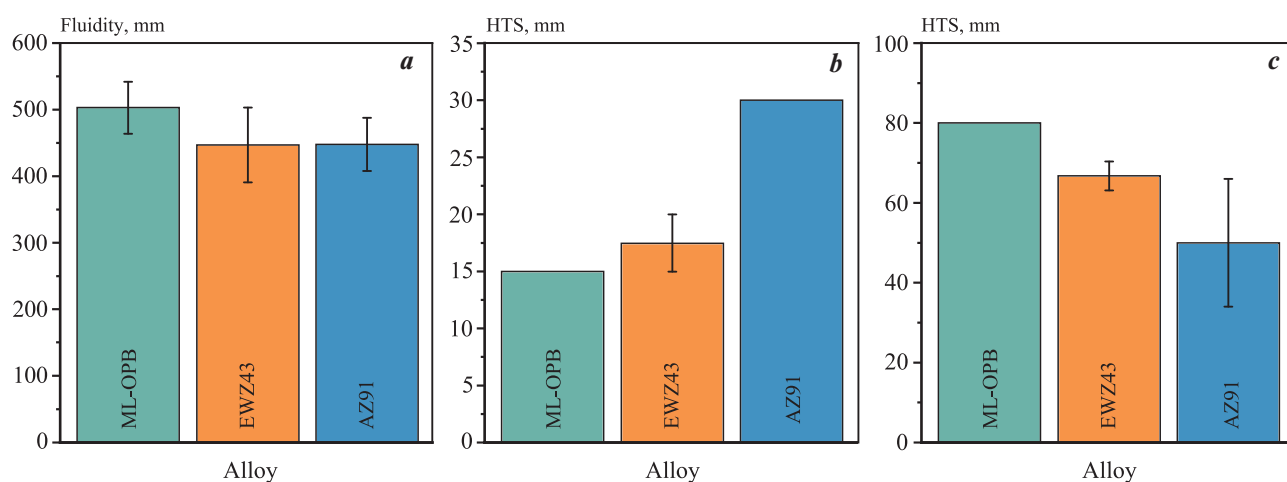


Fig. 5. Fluidity (*a*), hot tearing criterion obtained by the ring probe (*b*) and hot tearing criterion obtained by the «Dog-bone» test (*c*) for ML-OPB, EWZ43 and AZ91 alloys

Рис. 5. Жидкотекучесть (*a*), число горячеломкости по кольцевой пробе (*b*) и горячеломкость по пробе «Арфа» (*c*) для сплавов МЛ-ОПБ, EWZ43 и МЛ5

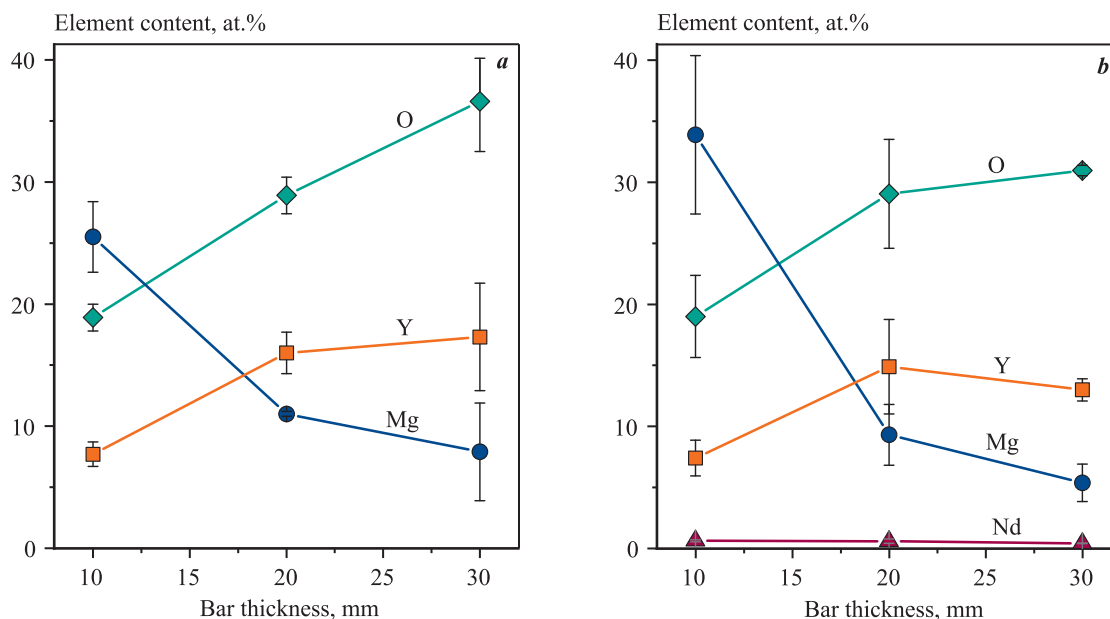


Fig. 6. The elements content in the oxide layer of ML-OPB (a) and EWZ43 (b) alloys bars with different thicknesses

Рис. 6. Содержание элементов в оксидной пленке брусков различной толщины для сплавов МЛ-ОПБ (a) и EWZ43 (b)

of cavities. When KBF_4 was used as an inhibitor, there were practically no ignition sources on the surface of the cylindrical ingots. This pattern was observed for both alloys studied.

We determined the ignition temperature for the alloys ML-OPB, EWZ43, as well as ML10. Fig. 7, a shows a typical heating curve of the ML-OPB alloy sample in air. It can be seen that during heating at 1077 °C there is a sharp increase in a temperature associated with additional heat release due to ignition of the sample. It should be noted that not in all cases the thermocouple readings were able to fix the ignition temperature, so at the same time we monitored the ignition visually.

Fig. 7, b shows the ignition temperatures of the ML-OPB, EWZ43 and ML10 alloys. It can be seen that the minimum ignition temperature of 878 ± 73 °C is observed for the ML10 alloy. The ML-OPB and EWZ43 alloys exhibit a higher value of 1022 ± 36 and 1054 ± 33 °C, respectively. Thus, the presence of Y in ML-OPB and EWZ43 alloys significantly increases their ignition temperature. Upon that, the EWZ43 alloy, which has a lower Y content than the ML-OPB alloy, exhibits the maximum ignition temperature. Apparently, the higher ignition temperature of the EWZ43 alloy is due to the presence of Nd. That is, Nd, as well as Ce [5, 8], contributes to the formation of a dense oxide film at lower Y concentrations.

Fig. 8, a illustrates a image of a cone-shaped ML-OPB alloy sample in the flame of a gas burner af-

ter 6 min from the beginning of the experiment. It can be seen that the sample has slightly changed its shape as a result of melting, but no ignition sources can be observed. Once 6 min had elapsed, the cone-shaped sample came into contact with the burner, whereupon it instantly lost its shape and flowed over the surface (Fig. 8, b). This suggests that the sample was primarily liquid and that its shape was preserved only due to the presence of a sufficiently strength oxide film. A similar behaviour was observed for the sample of alloy EWZ43, which, even after complete melting, could not show any ignition. As for the ML10 alloy, the average ignition time for it turned out to be 240 ± 63 s. The ignition sources on the cone-shaped sample made of the ML10 alloy can be seen in Fig. 8, c and d. Thus, it can be stated that the ignition resistance of the ML-OPB and EWZ43 alloys is extremely high and greatly exceeds that of the ML10 alloy.

Fig. 9 illustrates images of castings made of the ML-OPB, EZW43 and ML10 alloys, taken after 100 s from the start of ignition tests in the flame of a burner simulating an open fire on an aircraft. For the ML10 alloy (Fig. 9, c) the first ignition sources were observed 70 s after placing the casting in the burner flame. And already in the 100th second the multiple ignition sources can be seen. After the burner flame was turned off and the casting came into contact with the atmosphere, there was a bright flash and the ML10 alloy casting burned completely (Fig. 9, d). In the ML-OPB and

EWZ43 alloys (Fig. 9, *a* and *b*), no ignition sources appeared even after complete melting of the casting and melt spreading. It can be seen that the oxide films

formed on the ML-OPB and EWZ43 alloy castings are quite strength and partially preserve the shape of the casting, forming a kind of cover from which the alloy

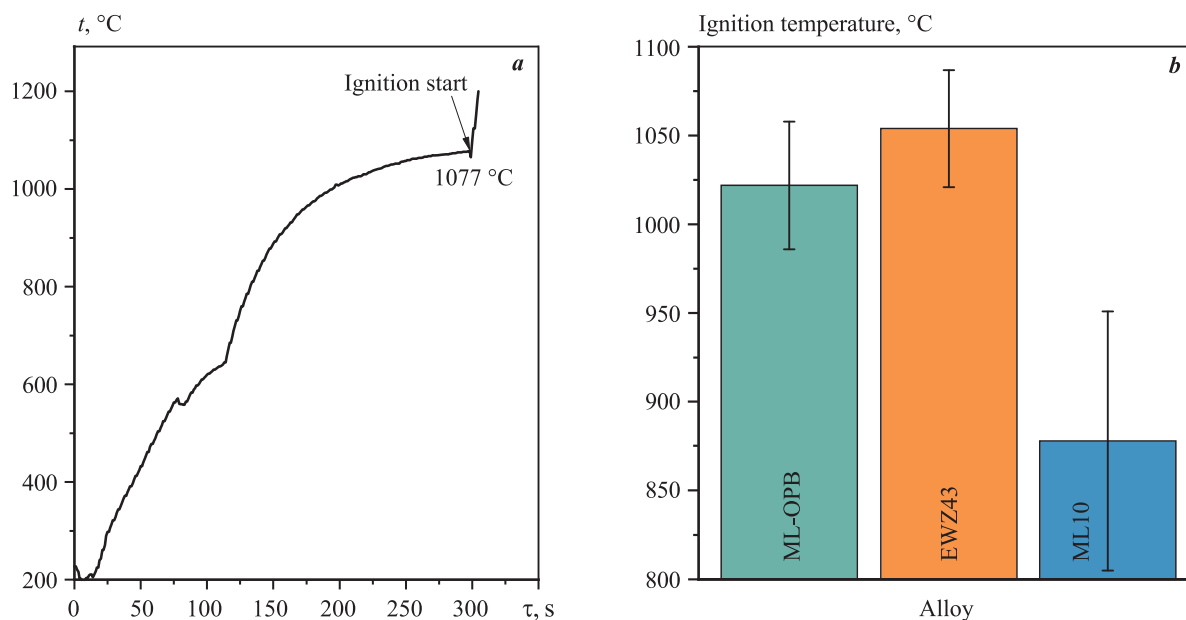


Fig. 7. The heating curve for ML-OPB alloy sample in air (*a*) and ignition temperature of ML-OPB, EZW43, and ML10 alloys samples (*b*)

Рис. 7. Кривая нагрева образца из сплава МЛ-ОПБ на воздухе (*a*) и температуры возгорания образцов из сплавов МЛ-ОПБ, EZW43 и МЛ10 (*b*)

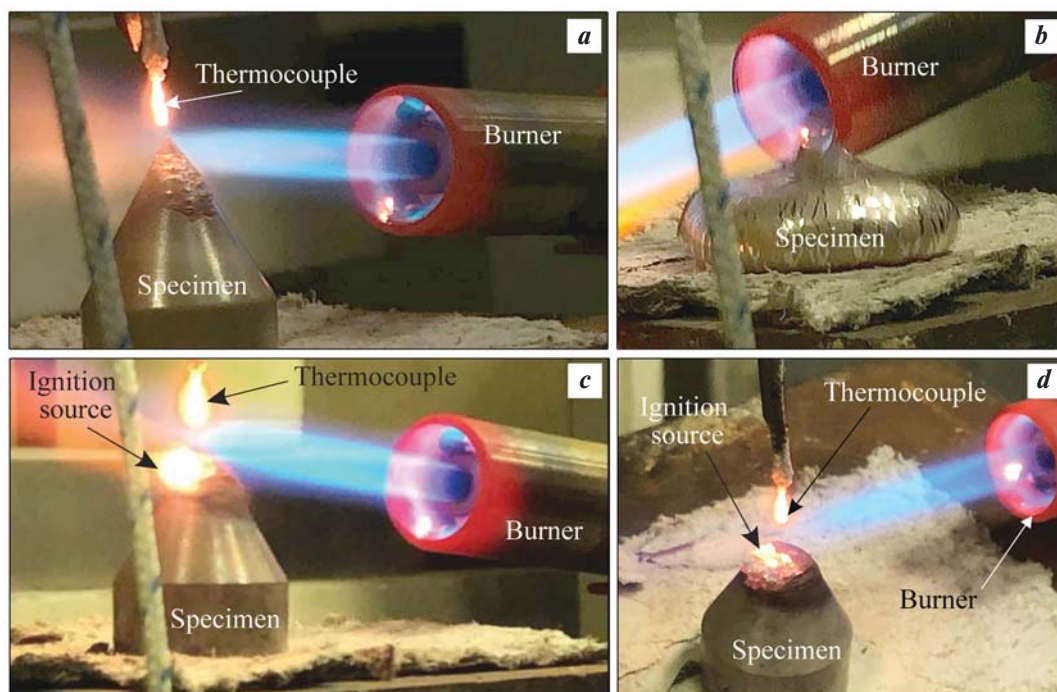


Fig. 8. The photographs of conical specimens made of ML-OPB (*a*, *b*) and ML10 (*c*, *d*) alloys during flammability tests in a gas burner flame

Рис. 8. Фотографии конусных образцов из сплавов МЛ-ОПБ (*a*, *b*) и МЛ10 (*c*, *d*) во время испытаний на возгорание в факеле газовой горелки

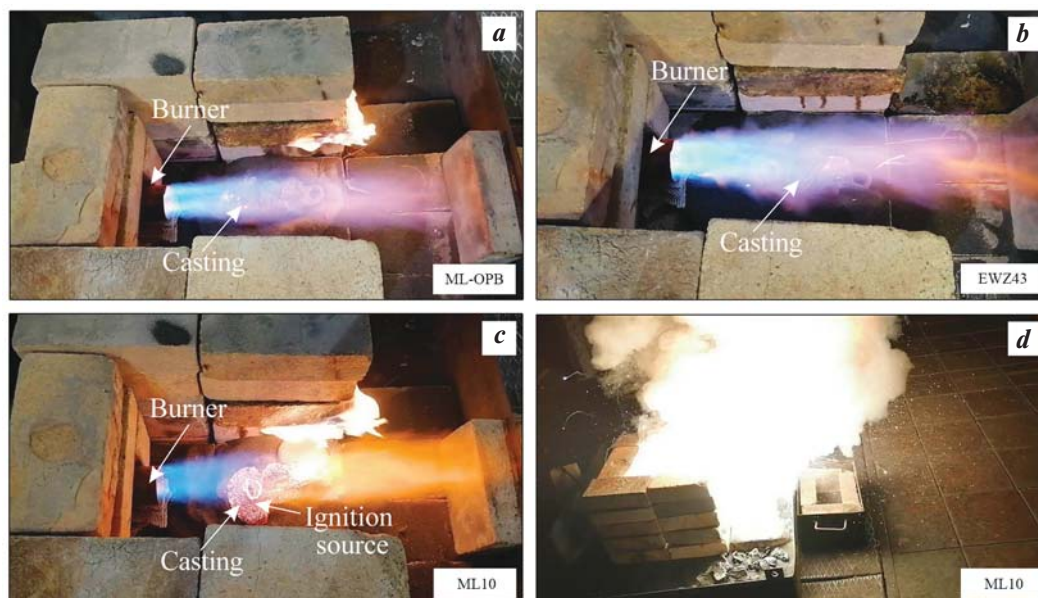


Fig. 9. The photographs of ML-OPB (a), EWZ43 (b) and ML10 (c) alloys castings after 120 s of flammability tests in a gas burner flame simulating an open fire on an aircraft, and combustion of a ML10 alloy casting at the end of the flammability experiment (d)

Рис. 9. Фотографии отливок из сплавов МЛ-ОПБ (a), EWZ43 (b) и МЛ10 (c) по прошествии 120 с испытаний на возгорание в пламени горелки, имитирующем открытый пожар на летательном аппарате, и горение отливки из сплава МЛ10 по окончании эксперимента (d)

flowed out. Upon that, the oxide films are kept heated to a high temperature by the burner flame and become glowing. After switching off the flame, the ML-OPB and EWZ43 alloys did not combust, unlike the ML10 alloy. These tests confirm that the ignition resistance of the ML-OPB and EWZ43 alloys is significantly higher than that of the ML10 alloy.

Conclusion

1. The microstructure of the ML-OPB alloy in the as-cast state consists of a α -Mg and LPSO-phase. As a result of HT, the morphology of the LPSO-phase changes to a lamellar one. Long-time holding at elevated temperature of samples made of the ML-OPB alloy ($t = 300\text{ }^{\circ}\text{C}$; $\tau = 500\text{ h}$) leads to the formation of precipitates on the grain boundary. The microstructure of the EWZ43 alloy consists of a α -Mg and the Mg_3Nd phase, which transforms into the $\text{Mg}_{41}\text{Nd}_5$ phase during the HT and its amount decreases significantly. The long-time holding at elevated temperature of the alloy also causes the formation of the grain boundary precipitates.

2. EWZ43 alloy significantly exceeds the tensile strength of the ML-OPB and ML10 alloys, but it exhibits small values of EI (about 5 % in T6 condition). The

tensile properties of ML-OPB and ML10 are similar, but ML-OPB exhibits higher EI. It was found that after a long-time holding at elevated temperature ($t = 300\text{ }^{\circ}\text{C}$; $\tau = 500\text{ h}$) the strength of the ML-OPB and EWZ43 alloys decreased, especially the EI for the ML-OPB alloy (twice). The reason for the decrease in properties is likely to be due to the precipitation of phases at the grain boundaries.

3. Long-time holding at elevated temperature of the alloys resulted in the formation of a Y-rich oxide film on the surface of the ML-OPB and EWZ43 alloy samples. Likewise, the Yb and Nd oxides in the ML-OPB and EWZ43 alloys, respectively, can play a protective role.

4. The corrosion rates of the ML-OPB and EWZ43 alloys in a 3 wt.% NaCl solution, determined during immersion corrosion test by the amount of hydrogen released, were 6.9 and 6.3 mm/year, respectively, which is much higher than those of the most common magnesium alloys — AZ91 and ML10 (2.1 and 0.9 mm/year, respectively). Thus, castparts made of ML-OPB and EWZ43 alloys require additional protection against corrosion.

5. The fluidity of ML-OPB and EWZ43 alloys was not lower than that of commercial magnesium alloys. The HTS of the ML-OPB and EWZ43 alloys is comparable to the HTS of the shot freezing range ML10

alloy and lower than that of the long freezing range AZ91 alloy. The specified castability properties for the ML-OPB alloy were slightly higher than for the EWZ43 alloy.

6. The study of the interaction of the ML-OPB and EWZ43 alloys with the resin bonded sand revealed that a ignition inhibitor is not necessary for castings with a wall thickness of 30 mm or less. This high resistance of the oxide film is explained by the formation of yttrium oxide in the surface layers of the oxide film of the casting. At the same time, a ignition inhibitor (e.g. KBF_4) may be required when producing castings with a wall thickness of 60 mm or more.

7. The ignition temperature for the ML-OPB and EWZ43 alloys was 1022 and 1054 °C, respectively, which is significantly higher than that for the ML10 alloy (878 °C). Tests of the alloys in the flame of a gas burner on the cone-shaped samples indicated that the ML-OPB and EWZ43 alloys practically do not ignite and that the ML10 alloy ignites after a certain period of time, even prior to the complete melting of the sample. During the tests of standard aircraft castings of the “bracket” type, made of test alloys, in an open flame of a gas burner, simulating a fire on the aircraft, it was found that castings of the ML-OPB and EWZ43 alloys do not ignite until they are completely melted. At the same time the casting of the ML10 alloy ignite at temperatures close to the melting point.

References

1. Czerwinski F. Overcoming barriers of magnesium ignition and flammability. *Advanced Materials and Processes*. 2014; 172: 28–31.
2. Marker T.R. Development of a laboratory-scale flammability test for magnesium alloys used in aircraft seat construction. Scientific report No. DOT/FAA/TC-13/52. Springfield: National Technical Information Services (NTIS), 2014.
3. Tekumalla S., Gupta M. An insight into ignition factors and mechanisms of magnesium based materials: A review. *Materials and Design*. 2017; 113: 84–98. <https://doi.org/10.1016/j.matdes.2016.09.103>
4. Tan Q., Atrens A., Mo N., Zhang M.X. Oxidation of magnesium alloys at elevated temperatures in air: A review. *Corrosion Science*. 2016; 112: 734–759. <https://doi.org/10.1016/j.corsci.2016.06.018>
5. Fan J.F., Yang Ch.L., Han G., Fang S., Yang W.D., Xu B.S. Oxidation behavior of ignition-proof magnesium alloys with rare earth addition. *Journal of Alloys and Compounds*. 2011; 509 (5): 2137–2142. <https://doi.org/10.1016/j.jallcom.2010.10.168>
6. Aydin D.S., Bayindir Z., Hoseini M., Pekguleryuz M.O. The high temperature oxidation and ignition behavior of Mg–Nd alloys. Part I: The oxidation of dilute alloys. *Journal of Alloys and Compounds*. 2013; 569: 35–44. <https://doi.org/10.1016/j.jallcom.2013.03.130>
7. Zhao S., Zhou H., Zhou T., Zhang Z., Lin P., Ren L. The oxidation resistance and ignition temperature of AZ31 magnesium alloy with additions of La_2O_3 and La. *Corrosion Science*. 2013; 67: 75–81. <https://doi.org/10.1016/j.corsci.2012.10.007>
8. Fan J.F., Cheng S.L., Xie H., Hao W.X., Wang M., Yang G.C., Zhou Y.H. Surface oxidation behavior of Mg–Y–Ce alloys at high temperature. *Metallurgical and Materials Transactions A*. 2005; 36 (1): 235–239. <https://doi.org/10.1007/s11661-005-0155-7>
9. Cheng C., Lan Q., Wang A., Le Q., Yang F., Li X. Effect of Ca additions on ignition temperature and multi-stage oxidation behavior of AZ80. *Metals*. 2018; 8: 766. <https://doi.org/10.3390/met8100766>
10. Inoue S.I., Yamasaki M., Kawamura Y. Formation of an incombustible oxide film on a molten Mg–Al–Ca alloy. *Corrosion Science*. 2017; 122: 118–122. <https://doi.org/10.1016/j.corsci.2017.01.026>
11. Kim Y.H., Kim W.J. Flame-resistant Ca-containing AZ31 magnesium alloy sheets with good mechanical properties fabricated by a combination of strip casting and high-ratio differential speed rolling methods. *Metals and Materials International*. 2015; 21: 374–381. <https://doi.org/10.1007/s12540-015-4338-5>
12. Duyunova V.A., Leonov A.A., Trofimov N.V., Rostovtseva A.S. Effect of qualitative and quantitative ratios of rare-earth elements in a new fireproof cast magnesium alloy. *Russian Metallurgy (Metally)*. 2021; 2021 (11): 1409–1412. <https://doi.org/10.1134/S0036029521110033>
Дуюнова В.А., Леонов А.А., Трофимов Н.В., Ростовцева А.С. Особенности влияния качественного и количественного соотношения редкоземельных элементов в новом пожаробезопасном литейном магниевом сплаве. *Металлы*. 2021; (6): 34–38.
13. Konstantinov I.L., Baranov V.N., Sidelnikov S.B., Kulikov B.P., Bezrukikh A.I., Frolov V.F., Orelkina T.A., Voroshilov D.S., Yuryev P.O., Belokonova I.N. Investigation of the structure and properties of cold-rolled strips from experimental alloy 1580 with a reduced scandium content. *International Journal of Advanced Manufacturing Technology*. 2020; 109: 443–450. <https://doi.org/10.1007/s00170-020-05681-4>
14. Koltygin A.V., Bazhenov V.E., Belov V.D., Matveev S.V. Cast magnesium alloy: Pat. 2687359 (RF). 2018. (In Russ.).

- Колтыгин А.В., Баженов В.Е., Белов В.Д., Матвеев С.В. Литейный магниевый сплав: Пат. 2687359 (РФ). 2018.
15. Koltygin A.V., Bazhenov V.E., Khasenova R.S., Komissarov A.A., Bazlov A.I., Bautin V.A. Effects of small additions of Zn on the microstructure, mechanical properties and corrosion resistance of WE43B Mg alloys. *International Journal of Minerals, Metallurgy and Materials*. 2019; 26 (7): 858–868.
<https://doi.org/10.1007/s12613-019-1801-1>
 16. Zhu Y.M., Morton A.J., Nie J.F. The 18R and 14H long-period stacking ordered structures in Mg–Y–Zn alloys. *Acta Materialia*. 2010; 58 (8): 2936–2947.
<https://doi.org/10.1016/j.actamat.2010.01.022>
 17. Xu D., Han E.H., Xu Y. Effect of long-period stacking ordered phase on microstructure, mechanical property and corrosion resistance of Mg alloys: A review. *Progress in Natural Science: Materials International*. 2016; 26 (2): 117–128.
<https://doi.org/10.1016/j.pnsc.2016.03.006>
 18. Luo S.Q., Tang A.T., Pan F.S., Song K., Wang W.Q. Effect of mole ratio of Y to Zn on phase constituent of Mg–Zn–Zr–Y alloys. *Transactions of Nonferrous Metals Society of China*. 2011; 21 (4): 795–800.
[https://doi.org/10.1016/S1003-6326\(11\)60783-8](https://doi.org/10.1016/S1003-6326(11)60783-8)
 19. Xu D.K., Tang W.N., Liu L., Xu Y.B., Han E.H. Effect of W-phase on the mechanical properties of as-cast Mg–Zn–Y–Zr alloys. *Journal of Alloys and Compounds*. 2008; 461 (1–2): 248–252.
<https://doi.org/10.1016/j.jallcom.2007.07.096>
 20. Xu D.K., Tang W.N., Liu L., Xu Y.B., Han E.H. Effect of Y concentration on the microstructure and mechanical properties of as-cast Mg–Zn–Y–Zr alloys. *Journal of Alloys and Compounds*. 2007; 432 (1–2): 129–134.
<https://doi.org/10.1016/j.jallcom.2006.05.123>
 21. Bazhenov V.E., Saidov S.S., Tselovalnik Yu.V., Voropayeva O.O., Plisetskaya I.V., Tokar A.A., Bazlov A.I., Bautin V.A., Komissarov A.A., Koltygin A.V., Belov V.D. Comparison of castability, mechanical, and corrosion properties of Mg–Zn–Y–Zr alloys containing LPSO and W phases. *Transactions of Nonferrous Metals Society of China*. 2021; 31 (5): 1276–1290.
[https://doi.org/10.1016/S1003-6326\(21\)65577-2](https://doi.org/10.1016/S1003-6326(21)65577-2)
 22. Andersson J.O., Helander T., Huglund L., Shi P.F., Sundman B. Thermo-Calc and DICTRA, computational tools for materials science. *CALPHAD*. 2002; 26 (2): 273–312.
[https://doi.org/10.1016/S0364-5916\(02\)00037-8](https://doi.org/10.1016/S0364-5916(02)00037-8)
 23. Thermo-Calc software TCMG4: TCS Mg-based alloys database version 4 (accessed: 01.03.2022).
 24. Bazhenov V.E., Koltygin A.V., Sung M.C., Park S.H., Tselovalnik Y.V., Stepashkin A.A., Rizhskiy A.A., Belov M.V., Belov V.D., Malyutin K.V. Development of Mg–Zn–Y–Zr casting magnesium alloy with high thermal conductivity. *Journal of Magnesium and Alloys*. 2021; 9 (5): 1567–1577.
<https://doi.org/10.1016/j.jma.2020.11.020>
 25. Kirkland N.T., Birbilis N., Staiger M.P. Assessing the corrosion of biodegradable magnesium implants: a critical review of current methodologies and their limitations. *Acta Biomaterialia*. 2012; 8 (3): 925–936.
<https://doi.org/10.1016/j.actbio.2011.11.014>
 26. ASTM Standard G1-03. Standard practice for preparing, cleaning, and evaluating corrosion test specimens. West Conshohocken: ASTM International, 2011.
 27. ASTM Standard G102-89, Standard practice for calculation of corrosion rates and related information from electrochemical measurements. West Conshohocken: ASTM International, 2015.
 28. Bazhenov V.E., Pikunov M.V., Safronova A.A., Tselovalnik Yu.V. Hot-tearing susceptibility of Al–Zn alloys. *Russian Metallurgy (Metally)*. 2017; 2017: 711–717.
<https://doi.org/10.1134/S0036029517090026>
 - Баженов В.Е., Пикун М.В., Сафронова А.А., Целовальник Ю.В. Исследование горячеломкости сплавов системы Al–Zn. *Металлы*. 2017; (5): 37–44.
 29. Bazhenov V.E., Koltygin A.V., Titov A.Yu., Belov V.D., Pavlinich S.P. Influence of ignition inhibitors on the strength of resin bonded sand molds and the composition of the oxide film on the surface of ML19 alloy castings. *Liteinoe proizvodstvo*. 2019; (5): 8–14. (In Russ.).
Баженов В.Е., Колтыгин А.В., Титов А.Ю., Белов В.Д., Павлинич С.П. Влияние ингибиторов горения на прочность форм из ХТС и состав оксидной пленки на поверхности отливок из сплава МЛ19. *Литейное производство*. 2019; (5): 8–14.
 30. Koltygin A.V., Bazhenov V.E. Structure and properties of ML10 (NZ30K) magnesium alloy, used as a raw material for the castings production. *Tsvetnye metally*. 2017; (7): 68–72. (In Russ.).
Колтыгин А.В., Баженов В.Е. Структура и свойства магниевых сплавов МЛ10 (NZ30K), используемого в качестве шихты для производства отливок. *Цветные металлы*. 2017; (7): 68–72.
<https://doi.org/10.17580/tsm.2017.07.11>
 31. Bazhenov V.E., Sannikov A.V., Saidov S.S., Rizhskii A.A., Koltygin A.V., Belov V.D., Yudin V.A. Influence of the alloying elements content and cooling rate on the corrosion resistance of the ML10 alloy. *Liteinoe proizvodstvo*. 2020; (12): 13–18. (In Russ.).
Баженов В.Е., Санников А.В., Саидов С.С., Рижский А.А., Колтыгин А.В., Белов В.Д., Юдин В.А. Влияние содержания легирующих элементов и скорости охлаждения на коррозионную стойкость сплава МЛ10. *Литейное производство*. 2020; (12): 13–18.

- рости охлаждения на коррозионную стойкость сплава МЛ10. *Литейное производство*. 2020; (12): 13–18.
32. Bazhenov V.E., Koltygin A.V., Sung M.C., Park S.H., Titov A.Yu., Bautin V.A., Matveev S.V., Belov M.V., Belov V.D., Malyutin K.V. Design of Mg–Zn–Si–Ca casting magnesium alloy with high thermal conductivity. *Journal of Magnesium and Alloys*. 2020; 8 (1): 184–191.
<https://doi.org/10.1016/j.jma.2019.11.008>
33. Li C.Q., Xu D.K., Zeng Z.R., Wang B.J., Sheng L.Y., Chen X.B., Han E.H. Effect of volume fraction of LPSO phases on corrosion and mechanical properties of Mg–Zn–Y alloys. *Materials and Design*. 2017; 121: 430–441.
<https://doi.org/10.1016/j.matdes.2017.02.078>
34. StJohn D.H., Qian M., Easton M.A., Cao P., Hildebrand Z. Grain refinement of magnesium alloys. *Metallurgical and Materials Transactions A*. 2005; 36: 1669–1679.
<https://doi.org/10.1007/s11661-005-0030-6>
35. Jiang D.T., Mukherjee A.K. Spark plasma sintering of an infrared-transparent Y₂O₃–MgO nanocomposite. *Journal of the American Ceramic Society*. 2010; 93 (3): 769–773.
<https://doi.org/10.1111/j.1551-2916.2009.03444.x>

Information about the authors

Vyacheslav E. Bazhenov – Cand. Sci. (Eng.), Assistant Prof., Department of Foundry Technologies and Material Art Working (FT&MAW), National University of Science and Technology “MISIS” (NUST MISIS).
<https://orcid.org/0000-0003-3214-1935>
E-mail: V.E.Bazhenov@gmail.com

Ivan I. Baranov – Educat. Master, Department of FT&MAW, NUST MISIS.
<https://orcid.org/0000-0002-0465-7865>
E-mail: baranov.wania@yandex.ru

Anastasiya A. Lyskovich – Lab. Assistant, Department of FT&MAW, NUST MISIS.
<https://orcid.org/0000-0002-8490-4829>
E-mail: nastya719ls999@gmail.com

Andrei V. Koltygin – Cand. Sci. (Eng.), Assistant Prof., Department of FT&MAW, NUST MISIS.
<https://orcid.org/0000-0002-8376-0480>
E-mail: misistlp@mail.com

Andrei V. Sannikov – Cand. Sci. (Eng.), Assistant Prof., Department of FT&MAW, NUST MISIS.
<https://orcid.org/0000-0002-0517-7732>
E-mail: sannikov@ic-ltm.ru

Karen A. Kyaramyan – Head of Department of the Branch of Joint Stock Company “United Engine Corporation” “Research Institute of Technology and Organization of Engine Production” (JSC “UEC” “NIID”).
E-mail: k.kyaramyan@uecrus.com

Vladimir D. Belov – Dr. Sci. (Eng.), Head of Department of FT&MAW, NUST MISIS.
<https://orcid.org/0000-0003-3607-8144>
E-mail: vdbelov@mail.ru

Sergei P. Pavlinich – Dr. Sci. (Eng.), Director of the Branch of JSC “UEC” “NIID”.
E-mail: Pavlinich@uecrus.com

Информация об авторах

Вячеслав Евгеньевич Баженов – к.т.н., доцент кафедры литейных технологий и художественной обработки материалов (ЛТиХОМ) Национального исследовательского технологического университета «МИСИС» (НИТУ МИСИС).
<https://orcid.org/0000-0003-3214-1935>
E-mail: V.E.Bazhenov@gmail.com

Иван Ильич Баранов – учебный мастер кафедры ЛТиХОМ, НИТУ МИСИС.
<https://orcid.org/0000-0002-0465-7865>
E-mail: baranov.wania@yandex.ru

Анастасия Андреевна Лыскович – исследователь-лаборант кафедры ЛТиХОМ, НИТУ МИСИС.
<https://orcid.org/0000-0002-8490-4829>
E-mail: nastya719ls999@gmail.com

Андрей Вадимович Колтыгин – к.т.н., доцент кафедры ЛТиХОМ, НИТУ МИСИС.
<https://orcid.org/0000-0002-8376-0480>
E-mail: misistlp@mail.ru

Андрей Владимирович Санников – к.т.н., доцент кафедры ЛТиХОМ, НИТУ МИСИС.
<https://orcid.org/0000-0002-0517-7732>
E-mail: sannikov@ic-ltm.ru

Карен Абовович Кярамян – начальник отдела филиала АО «ОДК» «НИИД».
E-mail: k.kyaramyan@uecrus.com

Владимир Дмитриевич Белов – д.т.н., заведующий кафедрой ЛТиХОМ, НИТУ МИСИС.
<https://orcid.org/0000-0003-3607-8144>
E-mail: vdbelov@mail.ru

Сергей Петрович Павлинич – д.т.н., директор филиала АО «ОДК» «НИИД».
E-mail: Pavlinich@uecrus.com

Contribution of the authors

V.E. Bazhenov – conceptualization, analysis of the experimental results, writing of the manuscript.

I.I. Baranov – realization of experiment, analysis of the experimental results.

A.A. Lyskovich – realization of experiment, analysis of the experimental results.

A.V. Kolygin – scientific guidance, review and editing of the manuscript.

A.V. Sannikov – realization of experiment, analysis of the experimental results.

K.A. Kyaramyan – formulation of the aims and objectives of the study, provision of resources.

V.D. Belov – supervision, review and editing of the manuscript.

S.P. Pavlinich – supervision, review and editing of the manuscript.

Вклад авторов

В.Е. Баженов – формирование основной концепции, обработка результатов исследований, написание текста статьи.

И.И. Баранов – проведение экспериментов, обработка результатов исследований.

А.А. Лыскович – проведение экспериментов, обработка результатов исследований.

А.В. Колтыгин – научное руководство, редактирование текста статьи.

А.В. Санников – проведение экспериментов, обработка результатов исследований.

К.А. Карамян – формулировка цели и задачи исследования, обеспечение ресурсами.

В.Д. Белов – общее руководство, редактирование текста статьи.

С.П. Павлинич – общее руководство, редактирование текста статьи.

The article was submitted 18.05.2022, revised 22.08.2022, accepted for publication 24.08.2022

Статья поступила в редакцию 18.05.2022, доработана 22.08.2022, подписана в печать 24.08.2022